# Journal of Materials Chemistry A

Accepted Manuscript

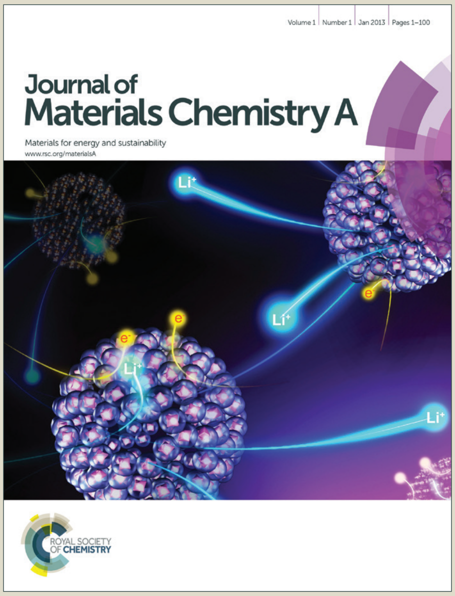

ROYAL SOCIETY OF CHEMISTRY

www.rsc.org/materialsA

Journal of Materials Chemistry A RSCPublishing

ARTICLE

Cite this: DOI: 10.1039/x0xx00000x

Received 00th January 2012,
Accepted 00th January 2012

DOI: 10.1039/x0xx00000x

www.rsc.org/

# Facile Fabrication and Photoelectrochemical Properties of One Axis-Oriented NiO Thin Film with (111) Dominant Facet

Chang Woo Kim,[a] Young Seok Son,[a] Amol Uttam Pawar,[a] Myoung Jong Kang,[a] Jin You Zheng,[a] Vivek Sharma,[b] Paritosh Mohanty[b,*] and Young Soo Kang[a,*]

A facile method was developed for the fabrication of one axis-oriented p-type NiO monolayer film with (111) dominant facet on ITO glass. Initially, hexagonal nanoplates of $Ni(OH)_2$ were synthesized hydrothermally and these nanoplates were assembled to one axis oriented monolayered film on ITO glass. Mesoporous NiO with pore diameter of ca. 1.7 nm were obtained by heating the single crystalline $Ni(OH)_2$ monolayered film at 400 °C for 3 hrs in air. The (111) facet oriented NiO thin film shows an enhanced photocathodic electrode activity with the photocurrent density of 0.38 mA/cm$^2$ at the potential of -0.9 V vs Ag/AgCl. For the first time, we address that the mesoporous NiO thin film with exposed (111) dominant facet is fabricated and analyzed for photoelectrode.

## Introduction

Organizing nanostructures in a periodic manner draw great attention in recent times due to their extraordinary properties and potential applications in nanoelectronics, photonics, catalysis and so on. Recently photoelectrode with efficient solar energy conversion efficiency,[1] effective hole conductor[2] and extremely bright full color device[3] was carried out by organized nanostructure. Orienting nanostructures in the specific atomic environment with specific planes exposed to the surface have an altogether different thermodynamics compared to the randomly oriented nanostructures.[4-6] Atomic environment at specifically exposed surface with their atomic coordination interact intensively with the surrounding materials at their interface results in promising potential applications such as, heterogeneous catalysis, molecular adsorption and gas sensing etc.[7] The crystal facet engineering of semiconducting materials is related to their photoelectrochemical performances. The three dimensional arrangement of atoms at the surface of the single crystals with different dipole moment caused by the different number and arrangement of the atoms is responsible for the different degree of the surface photoactivity. The effect could also be calculated by density functional theory.[8]

Chen and coworkers reported the dramatic enhancement of photocurrent in anatase $TiO_2$ microcrystal with highly energetic exposed (001) facet compared with other facets.[5] Furthermore, research on the facet controlled microcrystal has been extended to visible responsive $TiO_2$ and $TiO_2$ photoelectrode has been extended by Prof. Liu.[9,10] Recently, several other materials have been reported with the faceted microstructures such as, {001}, {010}, and {101} facets of $TiO_2$ microcrystal,[8] facet-selective of ZnO nanorod,[11,12] $WO_3$ quasi-cubic crystal with {002}, {200} and {020} facets,[13] polyhedral $Cu_2O$ microcrystal,[14] dominant (040) facet of $BiVO_4$[15] and BiOCl nanosheet[16,17] with {001} facet.

Nickel oxide (NiO) is a p-type wide band gap semiconductor with band gap energy of 3.6-4.0 eV. It is one of the promising metal oxides used in photocatalysis, electrochemistry and electrochromics.[18-21] Very recently, NiO has been largely used as a cocatalyst because of its high p-type concentration and high hole mobility.[22] For the photo-electrochemical performance, it is very important to control the NiO microstructure such as, tube,[23] hollow spheres,[24] sheet[25] and flower[26] by synthesizing through various approaches. In most of the reports, the structure directing agents (SDA) are used for the control of these micro-/ nanostructures. Moreover, these controlled NiO microstructures have been rarely used for photoelectrode applications even though NiO is promisingly suitable for pseudocapacitor electrode applications because of their high theoretical specific capacitance and high chemical-thermal stability.[27] Photocathodic activity of NiO nanoparticles and mesoporous NiO have been rarely discussed in the literature.

In this study, we report a facile method for the preparation of mesoporous NiO thin film photoelectrode with one-axis oriented (001)-facet. No additives or no SDA were used and the reaction was carried out in aqueous medium. For one-axis orientation on transparent conducting oxide glass, the prepared hexagonal plate were loaded by polyethyleneimine (PEI) solution approach.[28]

## Experimental

### Hydrothermal Synthesis of $Ni(OH)_2$ Hexagonal Plate

$Ni(OH)_2$ hexagonal plates were synthesized by a hydrothermal method following our previous work with some modifications.[24] Typically, 5 mL of 2 M $Ni(NO_3)_2•6H_2O$ solution was added into 15 ml of 0.5 M NaOH solution with a vigorous stirring. The color of the resultant mixture gets turned green on adding the NaOH solution. Then the solution was transferred to a 30 mL Teflon-lined autoclave. The autoclave was sealed and kept at 180 °C for 8 hrs. The reactor was cooled down gradually to room temperature under water flow. The obtained pale green precipitate was washed by distilled water and ethanol several times and collected by centrifugation with a speed of 5000 rpm for 5 min. The fine powder was dried at 80 °C for 2 days. For comparison, each of 10 and 15 mL of 2 M $Ni(NO_3)_2$ solution was added into 10 and 5 ml of 0.5 M NaOH solution, respectively, and the experiments were carried out similar to the above procedure.

### Oriented NiO Thin Film on Transparent Conducting Oxide Glass

A finger rubbing method was used for the fabrication of monolayered thin film following the reported literatures with minor modification.[28,29] A 2 wt% polyethyleneimine (PEI) solution in ethanol was spin coated on cleaned ITO with speed 2500 rpm for 15 sec. Dry powder of hexagonal $Ni(OH)_2$ plate was gently rubbed on PEI coated ITO for monolayer film preparation. The as-prepared film was heat-treated at 400 °C for 3 hrs in air. In comparison with black colored NiO powder samples, monolayered NiO film was light greenish. For comparison of one-axis oriented NiO thin film, the same procedure was repeated for sample obtained from 5 and 10 mL of NaOH solution.

### Materials Characterization and Measurement of Photoelectrochemical Property

A field-emission scanning electron microscope (FE-SEM, Hitachi S-4300) operated at an acceleration voltage of 20 kV and transmission electron microscope (TEM, JEM-2100F) was carried out to investigate the microstructure of prepared precipitate and their thin film. Their crystal structure was analyzed using powder X-ray diffraction (XRD) using a Rigaku D/MAX-2500/pc diffractometer and specific surface areas using $N_2$ adsorption-desorption at 77.3 K in Quantachrome Autosorb-1. The optical properties including band gap of samples were monitored and determined from diffuse reflectance spectra (DRS) by Varian Cary 5000 UV-Vis-NIR Spectrophotometer (Agilent Technologies). The diffuse reflectance spectra were converted into the Kubelka-Munk function. Photoelectrochemical measurements were carried out with a Potentiostat/Galvanostat (Compactstat, Invium Technologies) in a conventional three-electrode cell using Pt wire as a counter electrode and an Ag/AgCl (in 3 M NaCl) electrode as a reference electrode. A 1.0 M of KOH aqueous solution was used as the electrolyte. The photocurrent vs potential (I-V) curves of each electrode were obtained under the dark and light illumination between -0.2 and -1.0 V vs Ag/AgCl at a rate of 10 mV/s. The incident photon-to-current conversion efficiency (IPCE, HS Technologies, Korea) was measured under light intensity of 100 $mW/cm^2$ (AM 1.5) after the absolute intensity of the monochromic incident light calibrated by a silicon photodiode (model BS-500, Bunkoukeiki Co., Ltd., Japan).

## Results and Discussions

Synthesis of some of the transition-metal hydroxides such as, Fe-, Co-, Ni- and Mn hydroxides with layered structure, in which positively charged metal hydroxides are alternatively arranged with anions together with water molecules[30] additives like SDA are very often used as anion and these reactions proceed as follows;[31,32]

$$M^{2+} (M = Mn, Co, Ni, Fe) + 2H_2O \rightarrow M(OH)_2 + 2H^+$$

$$\text{in the presence of SDA at} < 200\ ^{O}C \quad (1)$$

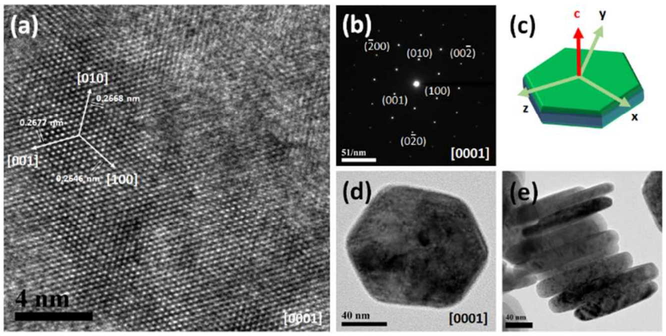

Figure 1. Microscopic observation of prepared $Ni(OH)_2$ hexagonal plate. (a) Lattice image from view of [0001], (b) SEAD pattern, (c) scheme of single crystal hexagonal plate, (d) typical TEM image of top and (e) typical TEM image of cross sectional view.

However, in the present approach, hexagonal $Ni(OH)_2$ plates were synthesized hydrothermally using $Ni^{2+}$ salt and NaOH solution, without using any additive. Well-defined facets with a truncated symmetric hexagonal shape have been observed in representative TEM image of specimen with edge length of 80 nm and thickness 30 nm as shown in Figure 1. The high resolution TEM (HRTEM, Figure 1a) and the selected area electron diffraction (SAED, Figure 1b) pattern viewed along the c-axis provide information about the growth direction of the plates. From the HRTEM image the lattice distance of 0.267

nm can measured and it matched with the direction of [100], [010] and [001] in hcp crystal structure. Thus, it can be confirmed that the (001) facet dominantly exposed on the surface of NiO plate. It was widely accepted that the SDA molecules can be adsorbed onto c-axis facet (plane) and suppress the growth direction of c axis as through bridging-bidentate adsorption.[30] As we have not used any SDA in our reaction, it can be conceived that the metal hydroxide with special facet come out of pH dependent reaction as was observed in our previous report.[24,33]

It was demonstrated by using thermogravimetric analysis in one of our earlier reports that the phase transition from $Ni(OH)_2$ to NiO and recrystallization occurs at 345 °C.[24] On heating the pale greenish $Ni(OH)_2$ sample at 400 °C for 3 hrs in air, black colored powder was obtained. Interestingly, as can be seen with the TEM images in Figure 2, there was no change in the hexagonal shape of the particles even on heating at that high temperature which induces the decomposition and as well as phase transition.

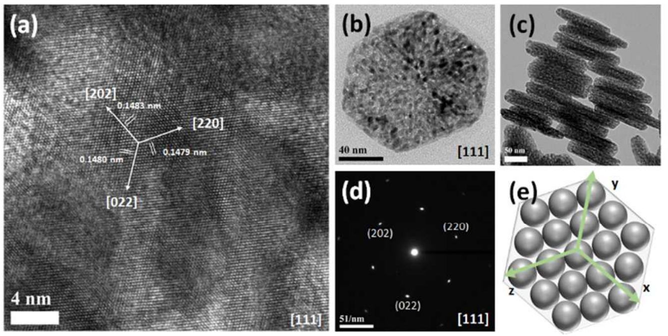

Figure 2. Microscopic observation of mesoporous NiO hexagonal plate. (a) Lattice image from view of [111], (b) typical TEM image of top, (c) typical TEM image of cross sectional view, (d) SEAD pattern and (e) scheme of mesoporous hexagonal plate.

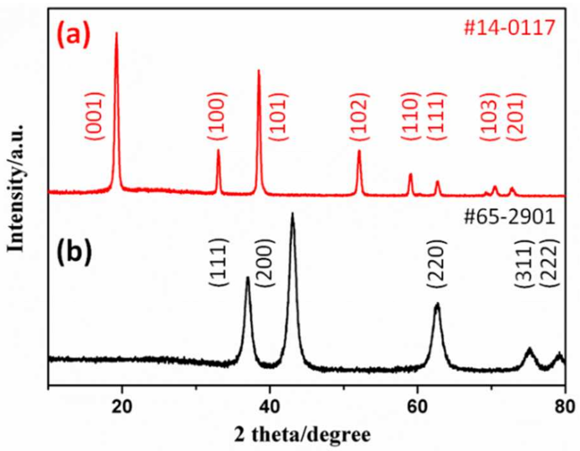

Figure 3. Powder XRD pattern of $Ni(OH)_2$ hexagonal plate (a) and mesoporous NiO (b).

But the particles became mesoporous in nature as can be seen with the TEM images in Figure 2 (a), (b), and (c). In the SAED pattern from Figure 2 (d), the lattice distance of all the direction is 0.148 nm and it is matched with (220) facet of NiO. It reveals that dominantly the mesoporous NiO hexagonal plates have exposed (111) facet on their surface. Figure 3 shows the XRD patterns of the $Ni(OH)_2$ and NiO samples. Several sharp diffraction peaks were observed in the 2θ range of 10 to 80 degree. These peaks were successfully indexed to the hexagonal crystal structure with space group for $Ni(OH)_2$, (PDF card #14-0117) and cubic crystal structure with symmetry for NiO (PDF card#65-2901).

The mesoporous nature of the specimen was studied and confirmed by $N_2$ adsorption/desorption analysis in Figure 4. As observed in the isotherms, the $Ni(OH)_2$ sample show non-porous behavior as no hysteresis was observed. The specific surface area of the sample calculated from the BET equation is 47.8 $m^2$/g. However, as expected the NiO sample shows a small hysteresis with H1-type loop.[34] The BET specific surface area of the sample was calculated to be 230 $m^2$/g. Furthermore, the NiO sample has a narrow BJH pore size distribution (PSD) centered at 1.7 nm.[35] It can further be clearly seen with the PSD the non-porous nature of the $Ni(OH)_2$ specimen.

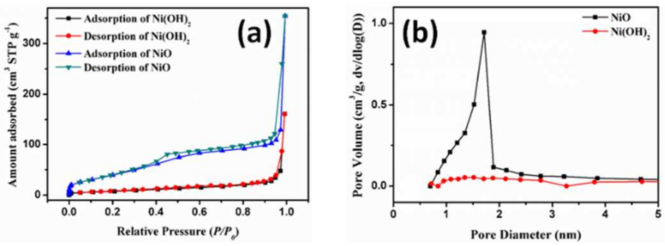

Figure 4. $N_2$ adsorption/desorption isotherms (a) and pore size distribution (b) of $Ni(OH)_2$ hexagonal plate and mesoporous NiO.

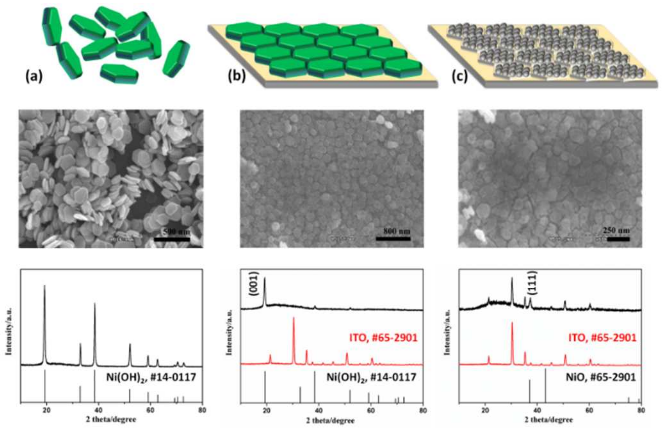

Figure 5. Schematic drawings, SEM images and XRD pattern of $Ni(OH)_2$ crystals (a), monolayer $Ni(OH)_2$ film (b) and oriented NiO film (c).

The single crystalline nature of the NiO hexagonal nanoplates with dominant oriented facets and the presence of mesopores prompted us to study the photocathodic properties. One-axis oriented thin film of NiO single crystals was fabricated by finger rubbing the specimen on ITO. Initially, PEI solution is coated on ITO glass and dried. The imine group in PEI formed the covalent bond with oxygen on the ITO surface, and resulted in the formation of film of metal oxide on the substrate surface. As shown in Figure 5, by finger-rubbing

$Ni(OH)_2$ powders on ITO glass, hexagonal $Ni(OH)_2$ plates were assembled to form a monolayer thin film. It is presumed that the (001) plane on hexagonal plate of $Ni(OH)_2$ is bonded to the imine linkage of the substrate and the facet is exposed with (001) plane.

The geometry of the hexagonal $Ni(OH)_2$ plates with dominant {001} facets allowed to have a close-packed c-axis oriented monolayer film. This can be confirmed from the SEM image and the XRD pattern of the film shown in Figure 5 (b). The XRD pattern reveals the enhanced intensity of the (001) diffraction peak compared to the powder XRD pattern. The NiO thin film that was obtained by heating the $Ni(OH)_2$ film has neither lost the orientation nor the single crystallinity. The thin film XRD pattern of the NiO as shown in Figure 5 (c) shows an enhanced intensity of the (111) peak of NiO film. This indicates that the hexagonal NiO plate has a dominant {111} facets faced upward and [111] c-axis is oriented with monolayered film arrays.

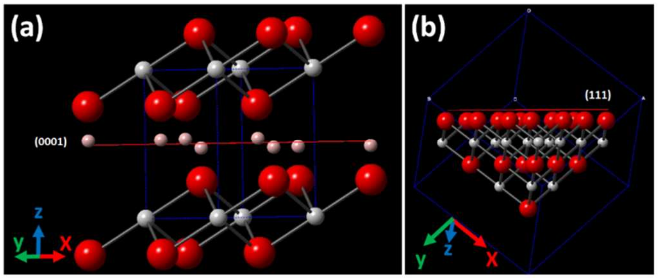

Figure 6. 3-Dimensional structure of $Ni(OH)_2$ plate unit cell with space group $P\overline{3}m1$ (a) and NiO plate unit cell with symmetry $Fm\overline{3}m$ (oxygen atom; red color, Ni atom; white one, H atom: pink one).

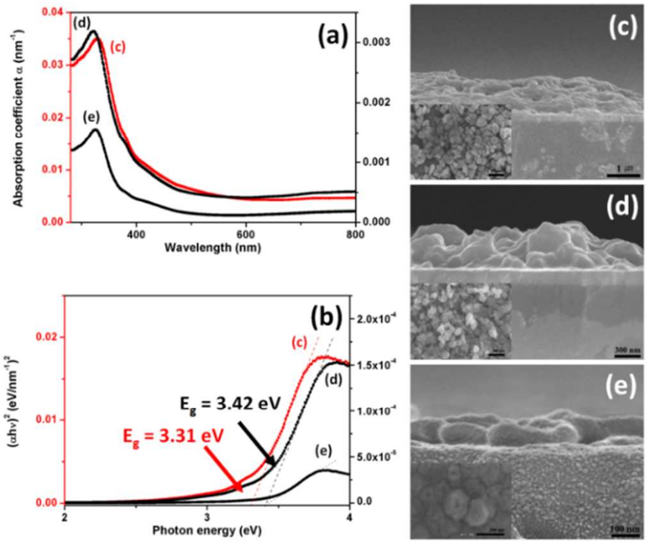

Figure 7. The optical absorption curves of NiO film (a), the $(\alpha h\nu)^2$ vs. hν plot (b) and typical SEM images of spherical typed NiO film (c), randomly oriented NiO film (d) and one axis-oriented NiO thin film (e).

With microscopic observation in Figure 5, (0001) plane as c axis is dominant in $Ni(OH)_2$ film on the ITO and also (111) plane is c axis in mesoporous NiO film on the ITO. Considering with atomic coordination at exposed facet, their atomic structure is related with surface reactivity. In Figure 6 (a), oxygen atom (white) is exposed in (0001) plane of $Ni(OH)_2$. While Ni atom (red) is terminated in (111) plane (Figure 6 (b)). We assumed that this surface structural feature show enhanced photocatalytic properties.

In order to understand the effect of the orientation in the NiO film properties and hence the applications, the optical properties of the (111) oriented NiO thin film was studied and compared with conventional and randomly oriented NiO films which was prepared using 10 mL and 15 mL of Ni salt solution (See Supporting Information, Figure S1). The optical contributions like light absorption coefficient and band gap energy obtained from the curves of $(\alpha h\nu)^2$ vs. hν were plotted in Figure 7 (a) and (b). By neglecting the factors like light scattering loss and Fresnel reflections, the light absorption coefficient would be determined as;

$$\alpha(E) = -\frac{1}{d}(\ln T_{normalized}(E)) \quad (2)$$

Where α(E) is an absorption coefficient, T(E) is transmittance and d is film thickness. From an inversion of α(E), the light incident length was calculated to be ca. 56 nm. The absorption coefficient decreases from 0.037 $nm^{-1}$ to 0.018 $nm^{-1}$ between oriented film and randomly oriented film.

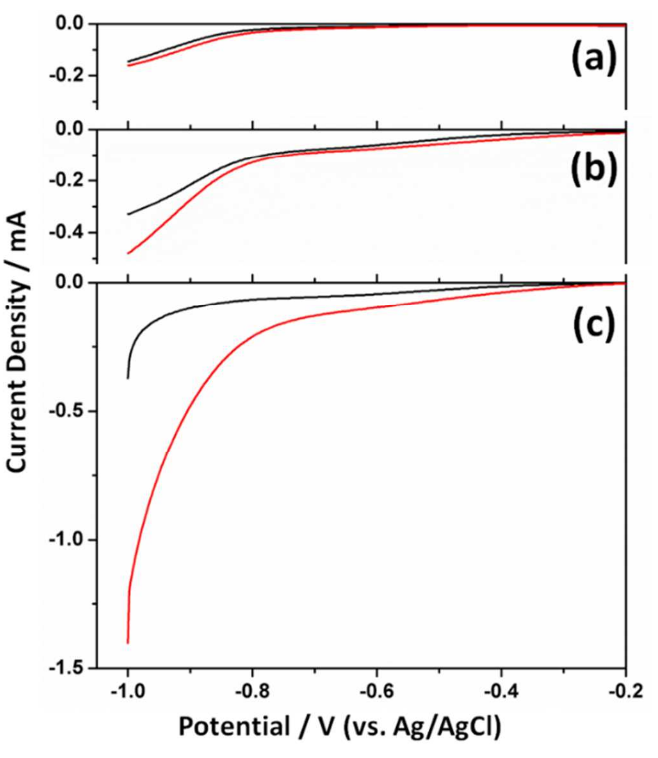

Figure 8. The photocathodic current density of spherical typed NiO film (a), randomly oriented NiO film (b) and (111) facet-oriented NiO thin film (c).

With a consideration of electronic transition by the absorption, Tauc-Davis-Mott relationship[36-38] is derived by the relation;

$$(\alpha h\nu)^2 = A(h\nu - E_g) \quad (3)$$

Where A is a constant, $E_g$ is the optical band gap of film and hν is photon energy. The extrapolated optical band gap of NiO thin film from the $(\alpha h\nu)^2$ versus hν plot is about 3.31 eV which is a red shift to that of bulk NiO with band gap energy of 3.50 eV. The energy gap for direct allowed transition in this film is about 3.31 eV.

Based on the optical properties, it is expected that (111) facet oriented NiO thin film show higher photoelectric activity compared to the other films. The photocathodic currents of three different films were checked in 1.0 M KOH (pH = 14) aqueous solution under one sun light illumination as shown in Figure 8. The thermodynamic potential for water reduction in this checking system can be calculated as ca. -1.0 V vs Ag/AgCl as the following formula.[39]

$$E_{RHE} = E_{Ag/AgCl} + E^0_{Ag/AgCl\ vs\ NHE} + 0.0591*pH \quad (4)$$

where $E_{RHE}$ is the converted potential vs RHE, 0 V vs RHE for the water reduction; $E_{Ag/AgCl}$ is the experimental potential measured vs Ag/AgCl reference electrode and $E^0_{Ag/AgCl\ vs\ NHE}$ is the standard potential of the Ag/AgCl vs NHE (0.207 V at 25 °C). The thermodynamic potential for water reduction is around -1.0 V vs Ag/AgCl. Herein, the photocathodic currents of the conventional thin film, randomly oriented and (111)-oriented NiO thin films at -0.9 V vs Ag/AgCl are ca. 0.38, 0.06 and 0.02 mA/cm$^2$, respectively. Thus, this effect can be attributed to the one-axis orientation with specific facet. Basically the stability of NiO would be critical because of photocorrosion like $Cu_2O$. The photocorrosion of NiO film was observed from the fact that their dark current increased as bias increased in photocurrent density (Figure 8). It indicates that some amount of photocorrosion is existing. Considering this point, test for stability was carried out as the photoresponse curve of (111) facet-oriented NiO thin film under 1 sun illumination at room temperature for 1 h (Figure S3).

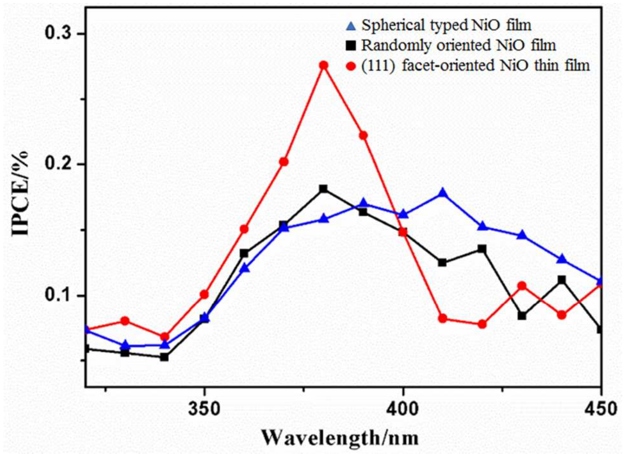

Figure 9. IPCE curves of spherical typed NiO film (blue), randomly oriented NiO film (black) and (111) facet-oriented NiO thin film (red).

The different photoelectrochemical properties of electrodes was shown with the incident photon to electron conversion efficiency (IPCE) which was carried out at -1.0 V vs Ag/AgCl under monochromic light illumination as shown in Figure 9.

$$\text{IPCE}(\%) = \frac{Isc(A)}{P(W)} \text{ X } \frac{1240}{\lambda(nm)} \text{ X } 100(\%) \quad (5)$$

Where $I_{SC}(A)$ is the photocurrent density, P(W) is the incident photon flux density and λ is wavelength. IPCE of randomly oriented film produce 0.17 %, but 0.27 % of IPCE was obtained in (111) oriented NiO film. IPCE of one-axis oriented film was higher than that of randomly oriented film.

As discussed earlier, the NiO hexagonal plate have (111) faces both top and bottom side and $(10\bar{1})$ plane as a six lateral facets. Surface geometry of $(10\bar{1})$ plane in NiO is terminated with equal number of Ni (white color) and O sites (red color) as shown in Figure 10 (a). Compared with $(10\bar{1})$ plane, more number of oxygen are terminated on (111) plane which can clearly be seen in Figure 10 (b). O-terminated sites is acted as dangling bonded sites and results in making (111) plane more polarized than that of $(10\bar{1})$ plane. This surface structural difference in (111)-oriented film where oxygen atom was exposed show an enhanced photocatalytic properties.

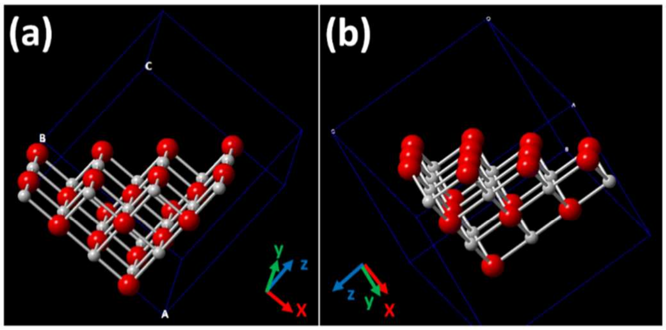

Figure 10. Ni-and O terminated sites in $(10\bar{1})$ plane and O terminated sites in (111) plane of NiO crystal structure (oxygen atom; red color, Ni atom; white one).

## Conclusions

In summary, we demonstrate for the first time the photocathodic properties of the mesoproous NiO thin film oriented with (111) facets. The film was fabricated by a rubbing method using hexagonal $Ni(OH)_2$ plates followed by heat treatment. Photocatalytic properties of NiO film was discussed in terms of the structural difference of the surface. $(10\bar{1})$ plane of NiO is terminated with of Ni and O atom and (111) plane is terminated with oxygen atom. At localized atomic scale in (111) facet, the number of exposed oxygen atom is more dominant than that of the others facet and result in enhanced photoelectrochemical activity. The fabricated (111) facet-oriented NiO film achieved photocurrent density of 0.38 mA/cm$^2$ at the potential of -0.9 V vs Ag/AgCl. It reveals their promising application in PECs.

## Acknowledgements

This work was supported by the Korea Center for Artificial Photosynthesis (KCAP) located in Sogang University funded by the Minister of Science, ICT and Future Planning (MSIP) through the National Research Foundation of Korea (No. 2009-0093885), and the Brain Korea 21 Plus Project 2014. P. Mohanty acknowledges India Korea research Internship programme (Code: INT/ROK/IKRI-6/2013).

## Notes and references

[a] Korea Center for Artificial Photosynthesis and Department of Chemistry, Sogang University, Seoul 121-742, Republic of Korea
[b] Department of Applied Science and Engineering, IIT Roorkee, Saharanpur Campus, Saharanpur 247001, U.P., India

† Electronic Supplementary Information (ESI) available: [Cross sectional SEM image and photoresponse data of NiO film]. See DOI: 10.1039/b000000x/

1 R. Nashed, P. Szymanski, M. El-Sayed, N. K. Allam, *ACS Nano,* 2014, **8**, 4915-4923.
2 W-C. Chen, Y-H. Lee, C-Y. Chen, K-C. Kau, L-Y. Lin, C-A. Dai, C-G. Wu, K-C. Ho, J-K. Wang, *ACS Nano,* 2014, **8**, 1254-1262.
3 W-C. Cho, S. S. Jo, I. Hwang, J. Sung, J. Seo, S-H. Jung, I. Bae, J. R. Choi, H. Cho, T. Lee, J. K. Lee, T-W. Lee, C. Park, *ACS Nano*, 2013, **7**, 10809-10817.
4 G. Liu, J. C. Yu, G. Q. (Max). Lu, H-M. Cheng, *Chem. Comm.*, 2011, **47**, 6763-6783.
5 J. Pan, G. Liu, G. Q. (Max). Lu, H-M. Cheng, *Angew. Chem. Int. Ed.,* 2011, **50,** 2133-2137.
6 A. Paracchino, V. Laporte, K. Sivula, M. Grätzel, E. Thimsen, *Nat. Mater.*, 2011, **10**, 456-461.
7 Y. Li, W. Shen, *Chem. Soc. Rev.,* 2014, **43**, 1543-1574.
8 G. Liu, H. G. Yang, J. Pan, Y. Q. Yang, G. Q. (Max). Lu, H-M, Cheng, *Chem. Rev.*, 2014, **ASAP DOI: 10.1021/cr400621z**.
9 G. Liu, L-C. Yin, J. Wang, P. Niu, C Zhen, Y. Xie, H-M, Cheng, *Energy Environ. Sic.*, 2012, **5,** 9603-9610.
10 C. Zhen, G. Liu, H-M, Cheng, *Nanoscale*, 2012, **4**, 3871-3874.
11 F-R. Fan, Y. Ding, D-Y. Liu, Z-Q. Tian, Z. L. Wang. *J. Am. Chem. Soc.*, 2009, **131,** 12036-12037.
12 J. Joo, B. Y. Chow, M. Prakash, E. S. Boyden, *Nat. Mater.*, 2011, **10**, 596-601.
13 Y. P. Xie, G. Liu, L. Yin, H-M. Cheng, *J. Mater. Chem.* 2012, **22**, 6746-6751.
14 S. Sun, X. Song, Y. Sun, D. Deng, Z. Yang. *Catal. Sci. Technol.*, 2012, **2**, 925-930.
15 D. Wang, H. Jiang, X. Zong, Q. Xu, Y. Ma, G. Li, C. Li, *Chem. Eur. J.,* 2011, **17**, 1275-1282.
16 D-H. Wang, G-Q. Gao, Y-W. Zhang, L-S. Zhou, A-W. Xu, W. Chen, *Nanoscale*, 2012, **4**, 7780-7785.
17 H. Cheng, B. Huang, Y. Dai. *Nanoscale*, 2014, **6**, 2009-2026.
18 Z. Huang, G. Natu, Z. Ji, P. Hasin, Y. Wu. *J. Phys. Chem. C,* 2011, **115**, 25109-25114.
19 L. Trotochaud, J. K. Ranney, K. N. Williams, S. W. Boettcher, *J. Am. Chem. Soc.*, 2012, **134,** 17253-17261.
20 G. A. Niklasson, C. G. Granqvist, *J. Mater. Chem.*, 2007, **17**, 127-156.
21 G. Wang, X. Liu, T. Zhai, Y. Ling, H. Wang, Y. Tong, Y. Li, *Nanoscale*, 2012, **4**, 3123-3127.
22 J. Ran, J. Zhang, J. Yu, M. Jaroniec, S. Z. Qiao, *Chem. Soc. Rev.,* 2014, **Advance Article DOI: 10.1039/C3CS60425J**.
23 X. Xu, J. Liang, H. Zhou, S. Ding, D. Yu. *RSC Adv.,* 2014, **4**, 3181-3187.
24 H. G. Cha, J. H. Sohn, Y. Park, K. J. Lee, M. H. Jung, J-W. Lee, W. Shin, M. J. Kang, D. Y. Kim, Y. S. Kang, *RSC Adv.,* 2012, **2**, 9786-9790.
25 J. Hu, K. Zhu, L. Chen, H. Yang, Z. Li, A. Suchopar, R. Richards, *Adv. Mater.*, 2008, **20**, 267-271.
26 L. X. Song, Z. K. Yang, Y. Teng, J. Xia, P. Du, *J. Mater. Chem. A*, 2013, **1**, 8731-8736.
27 S. Vijayakumar, S. Nagamuthu, G. Muralidharan, *ACS Appl. Mater. Interfaces,* 2013, **5**, 2188-2196.
28 J. S. Lee, Y-J. Lee, E. L. Tae, Y. S. Park, K. B. Yoon, *Science*, 2003, **301**, 818-821.
29 T. C. T. Pham, H. S. Kim, K. B. Yoon, *Angew. Chem. Int. Ed.*, 2013, **52**, 5539-5543.
30 P. Li, D. Wang, Q. Peng, Y. Li, *Cryst. Growth Des.*, 2013, **13**, 1949-1954.
31 K. K. Purushothaman, I. M. Babu, B. Sethuraman, G. Muralidharan, *ACS Appl. Mater. Interfaces*, 2013, **5**, 10767-10773.
32 M. Khairya, S. A. El-Safty, *RSC Adv.*, 2013, **3**, 23801-23809.
33 H. G. Cha, J. Song, H. S. Kim, W. Shin, K. B. Yoon, Y. S. Kang, *Chem. Commun.*, 2011, **47**, 2441-2443.
34 K. S. W. Sing, D. H. Everett, R. A. W. Haul, L. Moscou, R. A. Pierotti, J. Rouquerol, T. Siemieniewaska, *Pure and Applied Chemistry.*, 1985, **57**, 603-619.
35 J. H. De Boer, “The shapes of capillaries,” in The Structure and Properties of Porous Materials, in Proceedings of the 10th symposium, Colston Research Society University of Bristol, D. H. Everett, F. S. Stone (eds), Butterworths Science Publications, London, 1958, pp. 64-94.
36 J. Tauc, R. Grigorovici, A. Vancu, *Phys. Status Solidi.*, 1966, **15**, 627-637.
37 J. Tauc, (F. Abeles ed.), Optical Properties of Solids, North-Holland, 1972.
38 E. A. Davis, N. F. Mott, *Philos. Mag.*, 1970, **22**, 903-922.
39 J. C. Hill, K-S. Choi, *J. Mater. Chem. A*, 2013, **1**, 5006-5014.

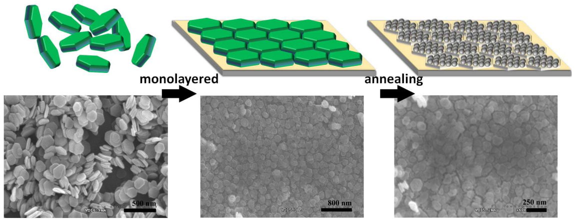

**One axis-oriented p-type NiO monolayer film** with (111) dominant facet on ITO glass was fabricated for photocathodic electrode.